Simulation of elastic-network relaxation: The $Si_{1-x}Ge_x$ random alloy

Matthew R. Weidmann and Kathie E. Newman
Department of Physics, University of Notre Dame, Notre Dame, Indiana 46556
(Received 23 September 1991; revised manuscript received 3 December 1991)

A method for relaxing a tetrahedral elastic network with length mismatch is developed. Systematic study of simulations finds close agreement with the predictions of analytic theory for mean values of nearest-neighbor bond lengths and reveals unexpected details in the full distributions in the limits $x \to 0, 1$. Application of the method to the problem of strain relaxation in bulk crystalline $Si_{1-x}Ge_x$ predicts trends in local structure that could be tested by experiment.

I. INTRODUCTION

Semiconductor alloys are solid solutions of two or more species of semiconducting compounds or elements. The atomic sizes of the constituents determine much about the structure and properties of an alloy. Lattice mismatches range from essentially zero for $Ga_{1-x}Al_xP$ to approximately 14% for $Sn_{1-x}Ge_x$. On the microscopic level, alloys mix two or more types of natural lengths for nearest-neighbor bonds. This mixing leads to internal strain as local structure relaxes to accommodate the mismatched lengths within the constraints of long-range crystalline order. A strong tendency to preserve individual bond lengths within alloys has been demonstrated by a number of experiments using EXAFS (extended x-ray absorption fine structure), a probe of local structure.[1–3]

A related problem that has been an active theoretical subject is the elastic behavior of classical networks composed of Hooke's law springs. Recent theoretical work[4] has pointed to a convergence of the problems of such networks and strain relaxation in semiconductor alloys.

The purpose of this paper is to present a model for simulating length-mismatched elastic networks with emphasis given to systems corresponding to real semiconductor alloys. The particular example chosen here is the $Si_{1-x}Ge_x$ alloy. This system is interesting because atomic site substitution occurs on both sublattices of the diamond structure, rather than on one as in ternary III-V and II-VI semiconductors, leading to different trends in structure. Additionally, there has been little experimental study of the local structural relaxation in bulk crystalline $Si_{1-x}Ge_x$, although there have been studies of amorphous[5,6] and epitaxial[7] alloys, as well as recent theoretical approaches to the problem.[4,8]

II. THEORY

A. Microscopic strain

The elastic network studied here is a classical system consisting of springs connecting points in a crystalline structure. The structure in this work corresponds to that of diamond, the underlying structure of most semiconductor alloys. For the example considered here, sites in the network can be occupied by atoms of two types, A (Si) or B (Ge), which leads to three natural bond-lengths, A-A, A-B, and B-B. The A-B bond length is taken to be the mean of the A-A and B-B lengths. The A-A bond will always be assumed shorter than the B-B bond throughout this paper. The possibility of vacancies or interstitials is not considered. Two types of Hooke's law springs are included, corresponding to a radial nearest-neighbor force and an angular next-nearest-neighbor force. The bond-stretching force drives the relaxation resulting from the bond-length mismatch while the bond-bending force resists distortion from the average crystal structure. The angle-preserving force is also necessary to stabilize the diamond structure, which has no resistance to shear with only radial nearest-neighbor forces present and is thus unphysical (as has been recently reiterated by Cai, Mousseau, and Thorpe[4]).

When viewed as a model of a semiconductor system, the elastic network is a rigid-ion or valence-force-field model. Such theories are well known in the study of semiconductors, the most widely used being Keating's model,[9] later extended by Martin.[10] The particular formalism used in this work is due to Kirkwood,[11] and more recently presented by Harrison.[12] In this approach, the Hooke's law forces are incorporated through the elastic strain energy (or Kirkwood potential) of the network, which is a sum over all distorted bonds and angles of energy terms quadratic in the distortions. The strain energy is written as

$$E = \sum_{i,j} \tfrac{1}{2} C_0 \left(\frac{d_{ij} - d_{ij}^0}{d_{ij}^0} \right)^2 + \sum_{ijk} \tfrac{1}{2} C_1 (\delta\theta_{ijk})^2 . \quad (1)$$

Here d_{ij}^0 is the natural length of the bond between atoms i and j, d_{ij} is the actual length of the bond and $\delta\theta_{ijk}$ is the deviation of angle centered on site j and terminated on the (nearest-neighbor) sites i and k from the perfect tetrahedral angle (109.47°). The force constants C_0 and C_1 are empirical parameters fit to the experimental elastic constants of the solid. The force constants used for mixed bonds and angles are given in Table I.

The network is relaxed by minimizing the total elastic strain energy with respect to variations in atomic posi-

TABLE I. Mixed-site force constants.

Bond A-B	$C_0 = (C_0^A + C_0^B)/2$
Angle A-A-B	$C_1 = (2C_1^A + C_1^B)/3$
Angle A-B-A	$C_1 = (C_1^A + C_1^B)/2$
Angle B-A-B	$C_1 = (C_1^A + C_1^B)/2$
Angle A-B-B	$C_1 = (C_1^A + 2C_1^B)/3$

tions, thus ensuring that the net force on a given site is zero. In this work it is assumed that distortions from the perfect crystal structure are small and so the deviations of atomic positions are dealt with in a linear first-order approximation. In the case of the $Si_{1-x}Ge_x$ alloy, this assumption is reasonable given the 3.8% bond-length mismatch. Each atomic site has full freedom to move in response to local forces, with the constraint that no bonds are broken or crossed. The final strain energy and all structural information are obtained from the relaxed configuration of the network.

Osgood and Harrison have recently questioned the validity of short-range force models that use parameters obtained from elastic constants, owing to the neglect of long-range electronic interactions.[13] We note here in response that structural trends depend primarily on geometry and local site occupation, found due to the presence of competing bond length and angle preserving forces (with the radial forces dominating), and not on the specific form of the microscopic interactions.

B. Supercell model

Simulation of the full random elastic network is accomplished with a supercell model.[14] Recent analytic work[4] has confirmed the importance of long-range adjustments in strain relaxation, even with only short-range forces involved, ruling out models based on clusters or small unit cells. A supercell model has the additional capability of including the effect of any local configuration of sites.

The typical supercell used contains $N = 1000$ sites of the diamond structure, with the dimensions of a large cube composed of 125 face-centered cubic unit cells (five regular cubes per side). Periodic boundary conditions apply at the edges of the supercell. The effects of superperiodicity are neglegible for this size cell. Lattice sites are occupied by atoms of type A or B, randomly placed to achieve the composition desired. The site distribution is thus simple binomial. The (relaxed) position of each site and the bond and angle types associated with it are explicitly retained in the model. Results are accumulated over many independent configurations of the cell.

Two methods for relaxing the supercell are available. The first is an exact solution of the problem (within the small displacements approximation), with all sites relaxed simultaneously. There are three independent parameters per site that describe local distortions and three additional parameters necessary for the relaxation of the lattice constants of the supercell. Technically, the problem reduces to solving a system of $3N + 3$ coupled linear equations and keeping track of all relevant site information.

TABLE II. Comparison of relaxation methods. The computer used was a Convex C240. For the approximate method, the total iterations and cpu time necessary for convergence to one part in 10^6 are given.

Cell size	Iterations	cpu seconds (approximate)	cpu seconds (exact)
64 sites	20	0.6	0.12
216 sites	45	1.3	4.6
512 sites	80	4.5	62
1000 sites	120	12.0	430
8000 sites	380	310	
27 000 sites	780	2100	
125 000 sites	1580	19 750	

The exact method is relatively slow in execution time and expensive in computer memory. It is impractical for $N > 1000$. An approximate method based on a simple physical picture of strain relaxation has been developed that avoids the practical difficulties of the "brute force" solution.

The approximate method for relaxing the supercell employs an iteration procedure based on a rigid-neighbor approximation. A single site is relaxed alone, with all neighbors held fixed. The strain energy terms used include only the four bonds and six angles associated with the site. This approximation builds on the notion, first advanced by Balzarotti *et al.*,[2] that strain relaxation can be understood in terms of the behavior of local tetrahedral clusters. The method avoids the previously mentioned limitations of cluster models because all clusters are simply part of the supercell.

The supercell is then relaxed sequentially, each site visited in turn (the order is irrelevant in this approximation), with all sites initially at average positions determined by the virtual-crystal approximation (VCA) for a given composition. The entire procedure is repeated until all atomic positions stabilize. Changes in atomic positions with iteration step converge quickly, becoming exponential after an initial number of steps. A 1000-site supercell requires 120 iteration loops to converge to a level of one part in 10^6, and 300 loops to achieve a level of one part in 10^{15}. This method is quite reliable when directly compared to the exact solution, the only detectable difference being a minor discrepancy in the limit of small x or $1 - x$ (see Sec. III C). It also requires far less computer time and memory, allowing much greater statistical accuracy and even the use of very large cells of 125 000 sites or more. The speeds of the exact and approximate methods are compared for several cell sizes in Table II. The approximate method is a useful tool for simulation with the exact method as a check.

In the following sections the method used to obtain results will always be indicated.

III. SIMULATION RESULTS

A. Systematics

Both approaches to the supercell model display the following systematic properties predicted by the analytic

theory of the random elastic network.[4] For the case of equal radial and angular force constants, $C_0^A = C_0^B$, $C_1^A = C_1^B$, the network displays several symmetries. The mean nearest-neighbor (NN) bond lengths A-A, A-B, and B-B are linear as a function of composition x. The strain energy is parabolic and symmetric about $x = 0.5$. Interestingly, the full distributions for the three nearest-neighbor bond lengths have identical functional shapes, with weights $(1-x)^2$ (A-A), $2x(1-x)$ (A-B), and x^2 (B-B). The centers of the distributions are of course different. The properties of distributions will be considered in more detail in Sec. III C.

In the limit $C_1 \rightarrow 0$, all bonds in the network attain their natural lengths and the strain energy tends to zero. Both versions of the supercell model reproduce this behavior for this special limiting case within the bounds of numerical accuracy.

The only discrepancy between the exact and approximate methods concerns the Vegard law behavior of the network. The exact method produces perfect adherence to Vegard's law for $C_0^A = C_0^B$, downward bowing for $C_0^A > C_0^B$ and upward bowing for $C_0^A < C_0^B$ (with $C_1^A = C_1^B$ always). Because of the condition of rigid neighbors, the approximate method does not allow the lattice constants of the supercell to relax and thus Vegard's law is imposed for all cases. In a random alloy, which is isotropic and thus has no preferred direction for lattice constant relaxation, this is not an important limitation.

B. $Si_{1-x}Ge_x$

This section details the simulation of the random alloy $Si_{1-x}Ge_x$ using the supercell model. The natural bond lengths used are 2.35 (Si) and 2.44 (Ge) Å and the force constants are $C_0^{Si} = 55.0$ eV, $C_0^{Ge} = 47.7$ eV, $C_1^{Si} = 3.2$ eV, $C_1^{Ge} = 2.8$ eV.[12] Results in this section for mean quantities were obtained from samples consisiting of one hundred independent configurations of a supercell with $N = 1000$ sites at each composition studied. Distributions were accumulated over one thousand configurations of such a supercell. The approximate relaxation method was used in both cases. The calculated strain energy for the random alloy is shown in Fig. 1.

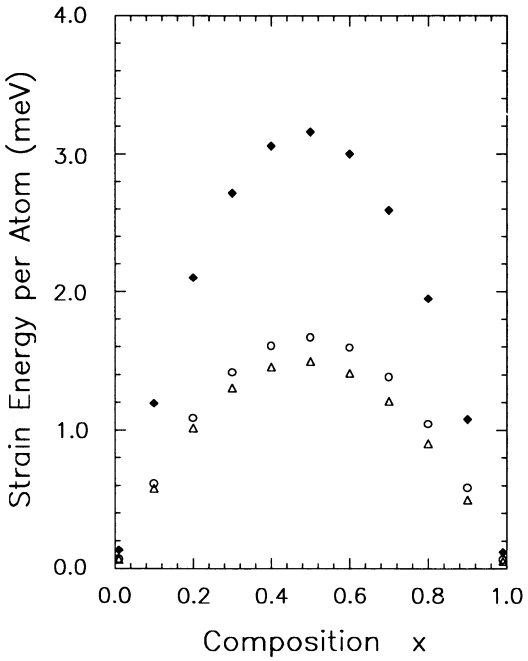

FIG. 1. Calculated total (diamonds), angular (circles), and radial (triangles) strain energies for random $Si_{1-x}Ge_x$ from the elastic network.

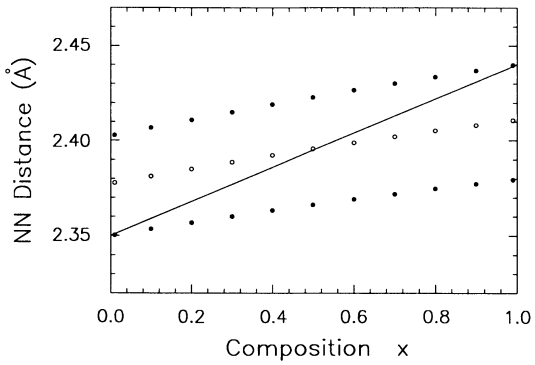

FIG. 2. Calculated mean nearest-neighbor bond lengths for $Si_{1-x}Ge_x$, Si-Si (lower solid circles), Si-Ge (open circles), Ge-Ge (upper solid circles). The solid line shows the predicted VCA bond length. Similar results are obtained in Refs. 4, 8, and 15.

Local structural quantities show several clear trends in the relaxed alloy. The mean NN bond lengths separate according to type, short Si-Si, intermediate Si-Ge, and long Ge-Ge, Fig. 2. The small curvature in the mean lengths as a function of composition is a result of the slight mismatch of force constants. The bonds are spread into distributions with the centers of each distribution having a value close but not exactly equal to the natural length. Figure 3 shows the full distributions for the NN bonds at $x = 0.2$. The distributions are close to Gaussian. Essentially identical results are obtained by Cai, Mousseau, and Thorpe[4] for the elastic network and by de Gironcoli, Giannozzi, and Baroni from Monte Carlo simulation of $Si_{1-x}Ge_x$.[8] Gregg has obtained similar results[15] using a cluster model described by Weid-

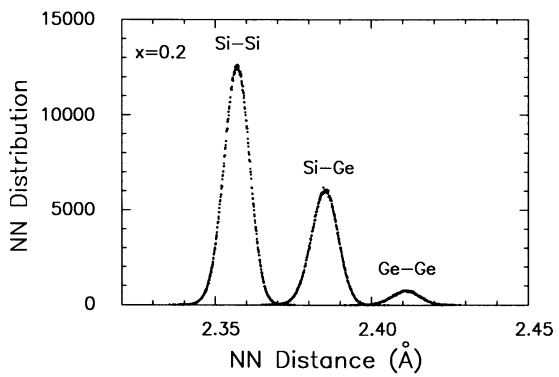

FIG. 3. Distributions for the nearest-neighbor bond lengths in $Si_{1-x}Ge_x$ at $x = 0.2$.

mann, Gregg, and Newman.[16] Our results for NN bond lengths in the impurity limits are comparable to those of Martins and Zunger.[17]

The mean deviations of bond angles from the perfect tetrahedral angle of 109.47° also show distinct trends, Fig. 4. There are three groupings here that separate according to the occupation of end-point sites. Angles with two Si end points are on average bent larger than ideal, those with mixed Si and Ge are smaller at small x and larger at large x, and those with two Ge are smaller for all x. The calculated distributions for all angle types at $x = 0.2$ are shown in Fig. 5. This behavior is in marked contrast to the case of amorphous alloys,[5] in which angular distributions are expected to center around $\delta\theta = 0$. The fourfold coordination of the underlying diamond crystal structure is the difference in this case.

These trends in local angular distortion can be understood in terms of relaxation around impurities near $x = 0$ and $x = 1$. For example, consider the Si-Si-Si and Si-Ge-Si angles. At low x the Si-Si-Si angle will obviously have $\delta\theta = 0$. At high x the three Si atoms making up this angle are isolated in the mostly Ge alloy. The lattice constant is close to that of pure Ge, so the unit of three Si sites will be stretched apart to fit into the larger Ge lattice, opening up the angle between them. The Si-Ge-Si angle will also be undistorted near $x = 0$ because the relaxation around the isolated central Ge site will be a uniform radial expansion, leaving the angles centered on the Ge site undisturbed. Near $x = 1$ the Si-Ge-Si angle is composed of two Si sites bonded to a common Ge within the mostly Ge alloy. The central Ge site will be pulled towards the two Si sites by the two short Si-Ge bonds, again opening up the angle. Similar arguments explain the trends in the other four angle types.

The calculated mean next-nearest-neighbor (NNN) distances appear in Fig. 6. These quantities are the separation between two sites that share a common nearest-neighbor site. The only direct coupling between the two end-point sites is angular. Here the two groupings depend not on the end points but on the central site, with

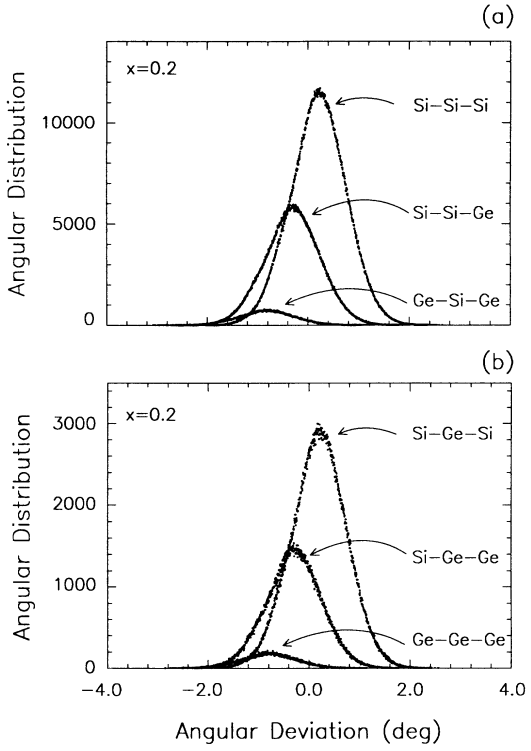

FIG. 5. Distributions for the (a) Si-Si-Si, Si-Si-Ge, and Ge-Si-Ge and (b) Si-Ge-Si, Si-Ge-Ge, and Ge-Ge-Ge bond angles at $x = 0.2$.

short distances centered on Si sites and long distances centered on Ge sites. This arrangement derives from the trends in the bond lengths and angles and can be explained by the law of cosines. If the NNN distance is c, the two NN bond distances are a and b, and the bond angle is θ, then $c^2 \cong a^2 + b^2 + \frac{2}{3}ab + \frac{\sqrt{8}}{3}\delta\theta$, after expanding for a small angular distortion $\delta\theta$ about $\theta = 109.47°$. As an example, consider the mean Ge-Si-Ge and Si-Ge-Si distances. Both are composed of the same type of bonds,

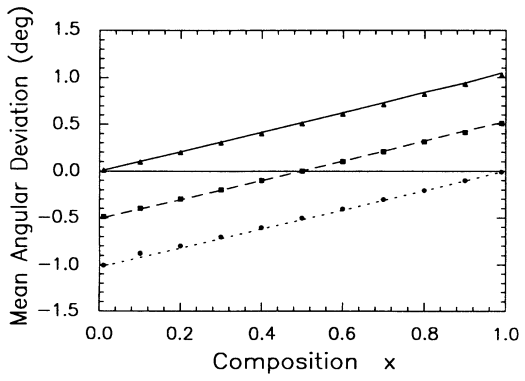

FIG. 4. Calculated mean bond-angle deviations for $Si_{1-x}Ge_x$. Si-Si-Si (triangles), Si-Si-Ge (squares), Ge-Si-Ge (circles), Si-Ge-Si (solid line), Si-Ge-Ge (long dashes), and Ge-Ge-Ge (short dashes).

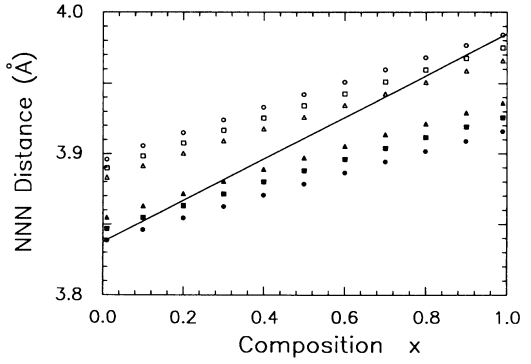

FIG. 6. Calculated mean second-neighbor distances for $Si_{1-x}Ge_x$. Si-Si-Si (solid circles), Si-Si-Ge (solid squares), Ge-Si-Ge (solid triangles), Si-Ge-Si (open triangles), Si-Ge-Ge (open squares), and Ge-Ge-Ge (open circles). The solid line represents the VCA prediction for second-neighbor distances.

Si-Ge, but the Ge-Si-Ge distance is short because its associated mean $\overline{\delta\theta}$ is negative and the Si-Ge-Si distance is long because of its positive $\overline{\delta\theta}$. The remaining NNN distances can be explained similarly. The distributions for all NNN distances at $x = 0.2$ are shown in Fig. 7. Unlike the nearest-neighbor distances, there is considerable overlap of the distributions.

C. Local structure in the dilute limits

We now return to the systematic properties of the elastic network. Simulation of elastic-network relaxation in the dilute concentration limits $x \approx 0$ and $1-x \approx 0$ reveals unexpected details in the local structure of the random alloy. A hypothetical random alloy $A_{1-x}B_x$ is studied, with several different choices of force constants and natural bond lengths always taken to be equal to those of Si and Ge. (For the main example, the force constants are chosen to be equal for simplicity and are approximately those of $Si_{1-x}Ge_x$.) Since the subject here is systematics, the exact relaxation method (employing a 512-site supercell) is used to ensure full precision, see below.

Consider the most obvious local structural quantity, the nearest-neighbor bond lengths. The full distributions for the bond lengths are approximately Gaussian in shape away from the dilute limits, but near $x \approx 0$ (or $1 - x \approx 0$) the distributions are clearly composed of distinct subpeaks. The emergence of the subpeaks as x changes from 0.08 to 0.02 is shown in Fig. 8, for a network with $C_0^A = C_0^B = 50.0$ eV and $C_1^A = C_1^B = 3.0$ eV. The effect is most clearly seen for the (dominant) A-A bonds, which occur with the highest probability as x becomes smaller, but the behavior of the (impurity) A-B and B-B bonds is exactly the same. The analytic theory[4] predicts that all three nearest-neighbor bond distributions should have identical functional shapes, and that is seen to hold in the simulation even in the limit of small x. The approximate relaxation method also reproduces this detailed structure with one small error: the centers of two subpeaks are shifted by ≈ 0.001 Å, due to partial truncation of long-range elastic displacements by the finite-iteration procedure.

The existence of the subpeaks can be attributed to the presence of impurity sites (B at small x, A at small $1-x$) in the first- and second-neighbor shells of the sites making up the type of bond in question. Figure 9 shows the two sites central to a bond (solid circles) and their first (lined circles) and second (open circles) neighbors. Throughout this section, first shell will denote any site that is nearest neighbor to either bond site, and second shell any site that is next-nearest neighbor (but not nearest) to a bond site.

Fully separated subdistributions were obtained by explicitly distinguishing A-A, A-B, and B-B bonds according to the number and location of impurity B sites in the first- and second-neighbor environments of each bond in the simulation samples. Figures 10–12 show these fully separated subdistributions for the dominant species A-

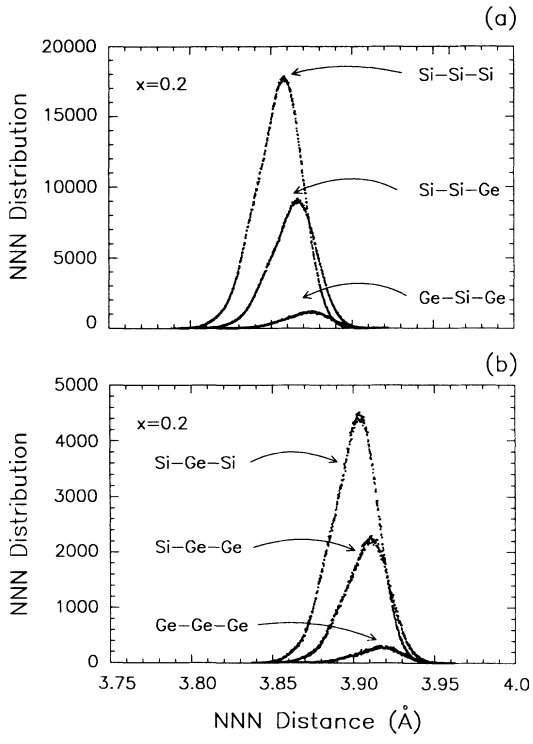

FIG. 7. (a) Distributions for the (a) Si-Si-Si, Si-Si-Ge, and Ge-Si-Ge and (b) Si-Ge-Si, Si-Ge-Ge, and Ge-Ge-Ge second-neighbor distances at $x = 0.2$.

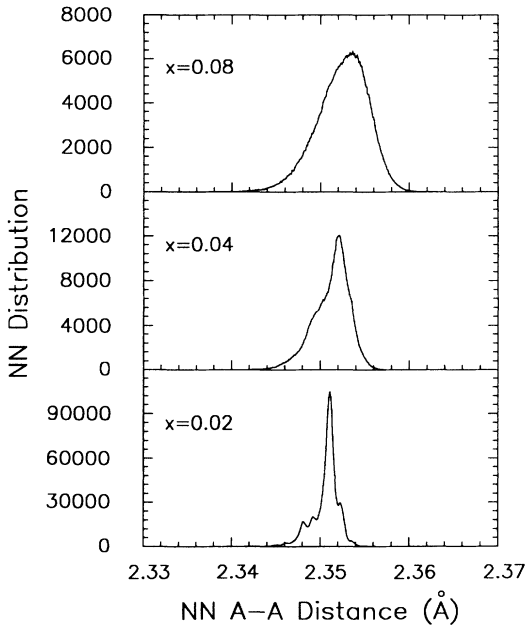

FIG. 8. Distributions for the nearest-neighbor A-A distances in a network $A_{1-x}B_x$ with force constants $C_0^A = C_0^B = 50.0$ eV and $C_1^A = C_1^B = 3.0$ eV at compositions $x = 0.08, 0.04, 0.02$. The subpeak structure emerges as the composition approaches the dilute limit. The samples at $x = 0.08, 0.04$ consisted of 256 000 sites. The sample at $x = 0.02$ was 1 024 000 sites. The individual cell size was 512 sites in all cases.

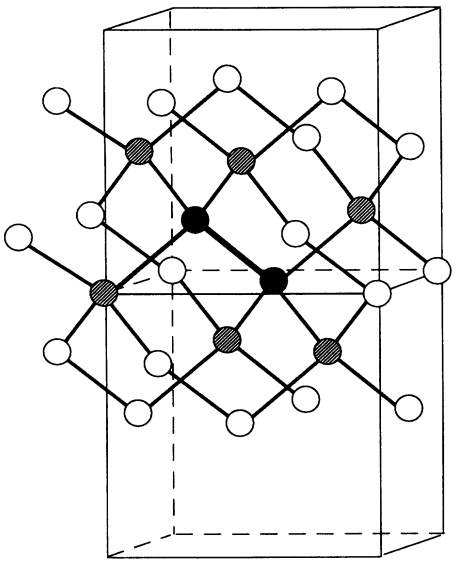

FIG. 9. The two sites (solid circles) central to a bond and the associated first (lined circles) and second (open circles) neighbor shells surrounding that bond. Also shown are the outlines of two face-centered cubes.

A bonds at $x = 0.02$ for the network with $C_0 = 50.0$ eV and $C_1 = 3.0$ eV (approximately $Si_{1-x}Ge_x$). Recall that the functional shapes of the impurity A-B and B-B distributions will be identical to that of the A-A distribution. All results were obtained from a sample consisting of 2000 512-site supercells. The vertical scale in Figs. 10–12 shows the number of bonds occurring in histogram bins 10^{-4} Å in width.

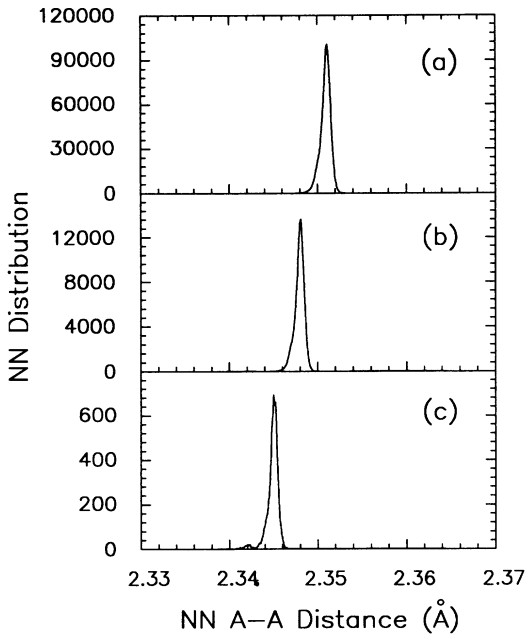

FIG. 10. Fully separated subdistributions of A-A nearest-neighbor distances in the network $A_{1-x}B_x$ ($C_0^A = C_0^b = 50.0$ eV, $C_1^A = C_1^B = 3.0$ eV) with no impurity B sites in the second shell around the central bond ($x = 0.02$). (a) No B sites in the first shell. (b) One B site in the first shell. (c) Two (or more) B sites in the first shell.

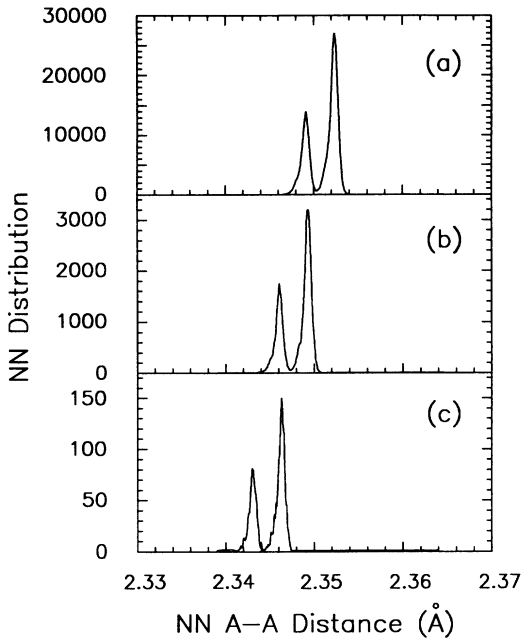

FIG. 11. Subdistributions of A-A distances with one B site in the second shell ($x = 0.02$). (a) No B sites in the first shell. (b) One B site in the first shell. (c) Two (or more) B sites in the first shell.

The subpeaks may be grouped into progressions distinguished by the number of impurities in the second shell, with scaling within the group according to the number of

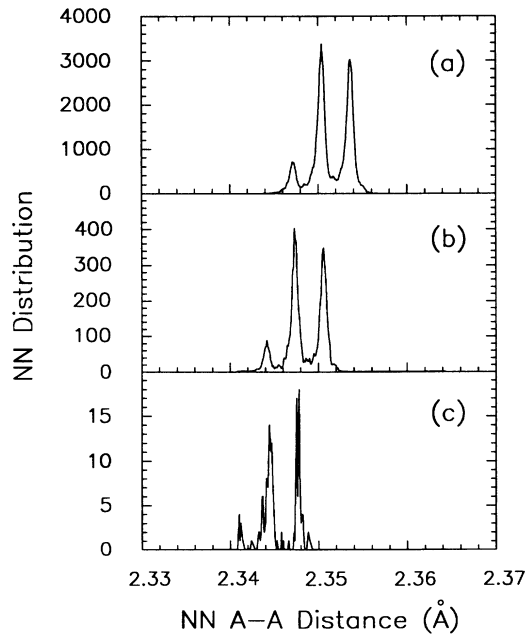

FIG. 12. Subdistributions of A-A distances with two (or more) B sites in the second shell ($x = 0.02$). (a) No B sites in the first shell. (b) One B site in the first shell. (c) Two (or more) B sites in the first shell.

impurities in the first shell. Figure 10(a) shows the peak for A-A bonds with no B in the first or second shell, Fig. 10(b) shows the peak for A-A bonds with a single B in the first shell, and Fig. 10(c) shows the peak for two or more B in the first shell (*none* in the second). The peaks decrease in height according to total number of B sites present (note the changing vertical scales) and the centers shift to shorter lengths, because more impurity B first neighbors compress the central bond more. All of the peaks consist of a dominant single mode and a small shoulder due to impurities in the third shell. There are no effects due to distinct geometrical configurations since all first-shell neighbors are equivalent. The small satellite peak in Fig. 10(c) is due to configurations with three (or more) B sites in the first shell.

The next progression of figures, 11(a)–11(c), show the subpeaks that occur with *one* B site in the second shell and zero, one, and two (or more) impurities in the first shell. The two peaks in Fig. 11(a) result from the two possible geometrical configurations for a single impurity in the second shell. The bond connecting the impurity to the first-neighbor shell is parallel to the central bond in six of the eighteen possible cases, resulting in two subpeaks with relative weights of six and twelve. Figures 11(b) and 11(c) show the related peaks arising from configurations with one B site in the second shell and one or more in the first shell. The centers of these peaks are again progressively shifted to smaller lengths and the total weights are scaled by the number of B sites present. The small background in Fig. 11(c) is due to bonds with three or more impurities in the first shell.

Finally, the peaks arising from configurations with *two* or more impurities in the second shell appear in Figs. 12(a)–12(c). There are three independent geometrical configurations for two B sites in the second shell, leading to the three main peaks in each of the diagrams. The background peaks in the diagrams are caused by three or more impurities in the second shell. The familiar shifting to shorter lengths and vertical scaling due to the presence of increasing numbers of impurities remains.

The finite widths of the subpeaks are real effects due to the surrounding medium beyond the second shell. The supercell model explicitly includes many shells of surrounding atoms and thus incorporates the long-range relaxations that produce the widths. The mean-square fluctuations $< d^2 > - < d >^2$ have been calculated at $x = 0.02, 0.04, 0.08, 0.16$ for the full A-A distribution and for the group of three subpeaks of the A-A distribution with *no* B sites in the second shell of the bond (these subpeaks appear in Fig. 10 for $x = 0.02$). Results for both are plotted as a function of $x(1-x)$ in Fig. 13. The mean-square fluctuation of the full distribution is proportional to $x(1-x)$, the same as a Gaussian, as demanded by the analytic solution.[4] Further, at each composition all of the subpeak fluctuations are equal within small statistical error, and also show a composition dependence of $x(1-x)$.

Typical errors in bond lengths due to neglect of second-order terms in the expansions of $d_{ij} - d_{ij}^0$ and $\theta_{ijk} + \delta\theta_{ijk}$ are on the order of 10^{-5} Å. This is much smaller than the range over which a single subpeak has appreciable weight.

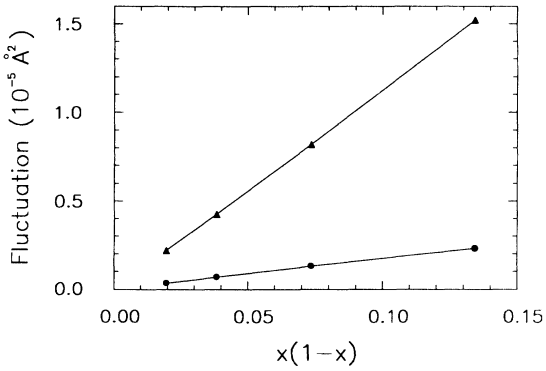

FIG. 13. Calculated mean-square fluctuations $< d^2 > - < d >^2$ for alloy $A_{1-x}B_x$ ($C_0 = 50.0$ eV, $C_1 = 3.0$ eV) as a function of $x(1-x)$. Triangles indicate the fluctuations of the full A-A distribution, circles indicate the fluctuations of the A-A subdistributions with *no* B sites in the second shell (see Fig. 10); in the latter case the three types of fluctuations are equal within an error smaller than the plot symbol size. The four points shown are for compositions $x = 0.02, 0.04, 0.08, 0.16$. The linear dependence on $x(1-x)$ is the same as a Gaussian.

(For the main example in this section at $x = 0.02$, the subpeaks have $\sqrt{< d^2 > - < d >^2} \sim 6 \times 10^{-4}$ Å.) The subpeak structure is clearly not an artifact of the linear first-order approximation used in relaxing the supercell.

For completeness we note here that at the other dilute limit, $(1-x) \approx 0$, a similar structure of subpeaks is found. The ordering of peaks is different, a mirror image of the low-x case, due to the fact that the impurities then have shorter bond lengths and the host has a longer natural length. Additionally, the full distributions of second-neighbor distances and bond angles show subpeak structure in the dilute limits, with the same origin. The computer simulations also indicate that the phenomenon of identical functional shapes for distributions extends to next-nearest-neighbor distances and bond angles, at all values of x (with force constants equal).

The structure of subpeaks is found to some degree for any physically realistic force constants, the only requirement being the presence of competing radial and angular forces. For example, Fig. 14 shows the subpeak structure at $x = 0.02$ and $x = 0.98$ for a network with a large mismatch of both radial and angular force constants. Because of the unequal force constants, the dominant peaks (A-A at $x = 0.02$ and B-B at $x = 0.98$) and impurity peaks (A-B in both cases) are no longer identical (although very nearly), and the low- and high-x structures are not exact mirror images. In the limit $C_1 \to 0$ the widths of the distributions vanish and the subpeak stucture disappears.

All subpeaks in the nearest-neighbor bond-length distributions can be explained by the number and geometrical configuration of impurity sites in the first- and second-neighbor shells of the bonds. This suggests an intuitive, physical explanation for the identical shapes of nearest-neighbor bond length distributions in the dilute limits. All types of bond, whether A-A, A-B, or B-B, respond

in the same way to the presence of *additional* impurities in the first- and second-neighbor environments, thus producing the same pattern of subpeaks in all three distributions. The apparently unusual equivalence of host and impurity distributions has a simple physical origin.

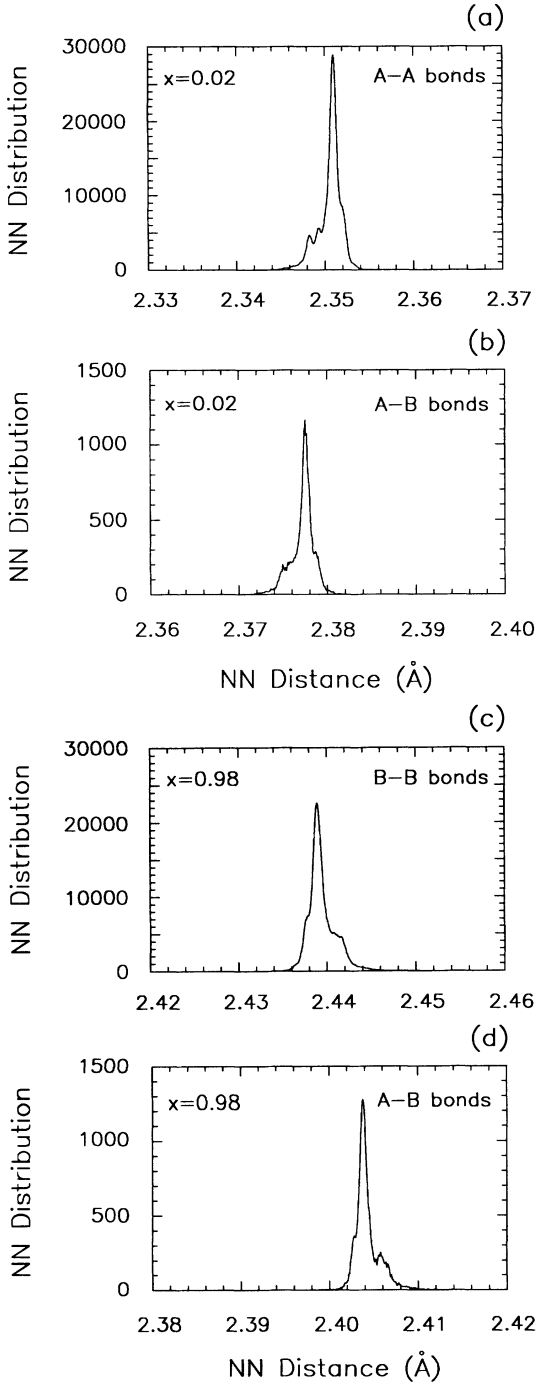

FIG. 14. Distributions for the nearest-neighbor distances for a network with $C_0^A = 50.0$ eV, $C_0^B = 25.0$ eV, $C_1^A = 3.0$ eV, $C_1^B = 1.0$ eV. The sample size was 256 000 sites (512-site cells) at both compositions. Note that the subpeak stucture is still clear despite the force-constant mismatch. (a) A-A distances at $x = 0.02$. (b) A-B distances at $x = 0.02$. (c) B-B distances at $x = 0.98$. (d) A-B distances at $x = 0.98$.

The occurrence of satellite peaks should not be confined to the system studied here, the diamond crystal structure populated by two atom types, but will be present in any tetrahedral network with length mismatch, including ternary or quatenary networks in the zinc-blende or wurtzite structures. In real semiconductor alloys, additional interactions such as charge transfer may complicate the effect. Nevertheless, given the overall success of spring models in describing local structure, it would be surprising to find a complete lack of structure in dilute-limit bond-length distributions in real semiconductor alloys.

IV. DISCUSSION

The supercell model described here is a reliable method for relaxing elastic networks with multiple natural lengths, as demonstrated by its close reproduction of the analytic solution of Cai, Mousseau, and Thorpe.[4] The rigid-neighbor relaxation method allows fast and extensive simulations whose accuracy can be carefully monitored. The method has great flexibility because the occupancy of sites can be completely controlled, permitting any local or long-range configuration to be studied. Generalization to many systems beyond the single example of random $Si_{1-x}Ge_x$ studied here is straightforward.

The model has demonstrated its usefulness by revealing a rich local structure present at the dilute concentration limits and providing a physical basis for understanding this structure and reconciling it with the requirements of the analytic solution. The satellite peak structure in the nearest-neighbor bond-length distributions seems surprising given the apparent simplicity of the analytic solution. Nevertheless the structure does conform to the theory and in fact helps explain why identical distribution shapes are preserved at low and high alloy-concentration limits (in the case of equal force constants). The detailed structure is also interesting because it necessarily follows that the full bond-length distribution is built up from the subdistributions at all compositions, although this is only apparent in the limiting cases.

It should be noted that in experimental studies it is usually the impurity bond distribution that is accessible, not the host. Recall, however, that all bond distributions will display subpeak structure, and since the force constants of real semiconductor alloys fall in a very limited range, host and impurity distributions will be very similar.

In dealing with the $Si_{1-x}Ge_x$ alloy in this work a random-site distribution has always been assumed. This is the common assumption for the bulk alloy in experiments and is supported by recent Monte Carlo simulations.[8] If the alloy is indeed random then experiments with EXAFS should see trends in the nearest-neighbor and next-nearest-neighbor environments very similar to the results predicted by our elastic network simulations. We know of no published EXAFS data for bulk crystalline $Si_{1-x}Ge_x$ at this time. EXAFS results from the Ge K edge for epitaxial Ge-Si layers grown on a Si(100) substrate do indicate that the Ge-Ge and Si-Ge bond lengths are conserved in the strained alloy layers.[7]

A more complete experimental study would be desirable for purposes of comparison.

ACKNOWLEDGMENTS

We acknowledge useful discussions with J. R. Gregg. We would like to thank M. F. Thorpe for providing copies of his papers prior to publication. We would also like to thank C. E. Bouldin for bringing his experimental work to our attention. We are grateful to R. A. Mayanovic and B. A. Bunker for critical reading of the manuscript. This work was supported by the United States Office of Naval Research under Contracts Nos. N00014-89-J-1198 and N00014-91-J-1062.

[1] J. C. Mikkelsen and J. B. Boyce, Phys. Rev. B **28**, 7130 (1983).
[2] A. Balzarotti, N. Motta, A. Kiesel, M. Zimnal-Starnawska, M. T. Czyzyk, and M. Podgorny, Phys. Rev. B **31**, 7526 (1985).
[3] W.-F. Pong, R. A. Mayanovic, B. A. Bunker, J. K. Furdyna, and U. Debska, Phys. Rev. B **41**, 8440 (1990).
[4] Y. Cai, N. Mousseau, and M. F. Thorpe (unpublished).
[5] L. Incoccia, S. Mobilio, M. G. Proietti, P. Fiorini, C. Giovannella, and F. Evangelisti, Phys. Rev. B **31**, 1028 (1985).
[6] Y. Nishino, S. Muramatsu, Y. Takano, and H. Kajiyama, Phys. Rev. B **38**, 1942 (1988).
[7] J. C. Woicik, C. E. Bouldin, M. I. Bell, J. O. Cross, D. J. Tweet, B. D. Swanson, T. M. Zhang, L. B. Sorenson, C. A. King, J. L. Hoyt, P. Pianetta, and J. F. Gibbons, Phys. Rev. B **43**, 2419 (1991).
[8] S. de Gironcoli, P. Giannozzi, and S. Baroni, Phys. Rev. Lett. **66**, 2116 (1991).
[9] P. N. Keating, Phys. Rev. **145**, 637 (1966).
[10] R. M. Martin, Phys. Rev. B **1**, 4005 (1969).
[11] J. G. Kirkwood, J. Chem. Phys. **7**, 506 (1939).
[12] W. A. Harrison, *Electronic Structure and the Properties of Solids* (Freeman, San Francisco, 1980).
[13] R. Osgood and W. A. Harrison, Phys. Rev. B **43**, 14 255 (1991).
[14] M. R. Weidmann and K. E. Newman, Bull. Am. Phys. Soc. **36**, 599 (1991).
[15] J. R. Gregg (unpublished).
[16] M. R. Weidmann, J. R. Gregg, and K. E. Newman, J. Phys. Condens. Matter **4**, 1 (1992).
[17] J. L. Martins and A. Zunger, Phys. Rev. B **30**, 6217 (1984).